 doi:10.20944/preprints202003.0385.v1

Atmospheric transport, a major pathway of microplastics to remote regions

N. Evangeliou[1,*], H. Grythe[1], Z. Klimont[2], C. Heyes[2], S. Eckhardt[1], S. Lopez-Aparicio[1], A. Stohl[1,3]

[1]Norwegian Institute for Air Research (NILU), Instituttveien 18, 2007 Kjeller, Norway.

[2]International Institute for Applied Systems Analysis (IIASA), 2361 Laxenburg, Austria.

[3]Department of Meteorology and Geophysics, University of Vienna, UZA II,
Althanstraße 14, 1090 Vienna, Austria

* Corresponding author: N. Evangeliou (Nikolaos.Evangeliou@nilu.no)

Preprints (www.preprints.org) | NOT PEER-REVIEWED | Posted: 27 March 2020 doi:10.20944/preprints202003.0385.v1

Abstract

In recent years, marine, freshwater and terrestrial pollution with microplastics has been discussed extensively, whereas atmospheric microplastic transport has been largely overlooked. Here, we present the first global simulation of atmospheric transport of microplastic particles produced by road traffic (TWPs – tire wear particles and BWPs – brake wear particles), a major source that can be quantified relatively well. We find a high transport efficiency of these particles to remote regions, such as the Arctic Ocean (14%). About 34% of the emitted coarse TWPs and 30% of the emitted coarse BWPs (100 kt yr^{-1} and 40 kt yr^{-1} respectively) were deposited in the World Ocean. These amounts are of similar magnitude as the total estimated terrestrial and riverine transport of TWPs and fibres to the ocean (64 kt yr^{-1}). Atmospheric transport of microplastics is thus an underestimated threat to global terrestrial and marine ecosystems and affects air quality on a global scale, especially considering that other large but highly uncertain emissions of microplastics to the atmosphere exist. High latitudes and the Arctic are highlighted as an important receptor of mid-latitude emissions of road microplastics, which may imply a future climatic risk, considering their affinity to absorb solar radiation and accelerate melting.

Preprints (www.preprints.org) | NOT PEER-REVIEWED | Posted: 27 March 2020 doi:10.20944/preprints202003.0385.v1

Main

Global annual plastic production reached 348 million tonnes in 2017[1] and, consequently, plastic pollution in freshwater[2], marine[3] and terrestrial[4] ecosystems has received a lot of attention recently. Plastics are released into the environment as macroplastic (>5 mm)[5], microplastic (1 µm to 5 mm)[6] and nanoplastic (<1 µm)[7] particles which can fragment into smaller sizes via photodegradation, physical abrasion, hydrolysis and biodegradation[8]. Plastics can affect coral reefs[9], marine[10] and terrestrial animals[11] as well as human health[12,13].

An important source of plastics is road traffic emissions. Kole et al.[14] reported global average emissions of tire wear particles (TWPs) of 0.81 kg year^{-1} per capita, about 6.1 million tonnes (~1.8% of total plastic production). Emissions of brake wear particles (BWPs) add another 0.5 million tonnes. TWPs and BWPs are produced via mechanical abrasion and corrosion[15,16].

Tires consist of a mix of elastomers such as rubber (natural and synthetic) and different additives[17]; TWPs are produced by shear forces between the tread and the road pavement, generating coarse particles[18], or by volatilization generating submicronic particles[19]. The wearing process depends on the type of tire, road surface and vehicle characteristics, as well as on the vehicle's state of operation[20].

Most car braking systems consist of frictional pairs made of a disc, a pad and a calliper. Brake linings consist of binders, fibres, fillers, frictional additives or lubricants and abrasives[21–23]. Thus, BWPs are a complicated mixture of metal and plastic. BWP emissions depend on the bulk friction material[21,24], on the frequency and severity of braking[25], speed, weight, condition and maintenance of the automobile[26] and the environmental conditions[21,27,28].

Transport of TWPs and BWPs via runoff and wash-out to marine and/or freshwater ecosystems has been studied[29,30]. However, very little is known about their dispersion in the atmosphere and where they are deposited, despite their health impacts in animals[9–11,31] and humans[12,32], possibly enhanced by absorbing toxic organic compounds and heavy metals[33]. Larger use of plastics results in more extensive consumption of fossil fuels and, in turn, in larger emissions of greenhouse gases[34] such as methane and ethylene[35]. Since TWPs and BWPs can be present at sizes smaller than 10 µm[36], they can long remain airborne and thus have been detected already in remote areas[37–39]. They are also light-absorbing and can decrease surface albedo of snow and ice accelerating melting [40].

Preprints (www.preprints.org) | NOT PEER-REVIEWED | Posted: 27 March 2020 doi:10.20944/preprints202003.0385.v1

Here, for the first time we examine atmospheric transport and deposition of TWPs and BWPs from road transport on a global scale. We have calculated TWP emissions based on two different approaches, one indirect and another using an emission model (see Methods). BWP emissions were only calculated with the emission model. For simplicity we often refer to these particles jointly as "road microplastics" throughout this paper. Even though they contain components other than plastics (e.g., metals), plastics are the dominant component especially for TWPs. We also speak of microplastics, since we only consider the particles smaller than 10 µm, which can long remain airborne.

Annual global emissions of road microplastics

TWP emissions were calculated using two different approaches, (a) one based on detailed information of TWP emissions in Northern Europe and extrapolation using a CO_2 ratio method, and (b) one based on the GAINS model (see Methods). Considering that TWP emissions are very similar for the two methodologies used (3434 kt and 2380 kt), we report the average values. Uncertainties were calculated based on different assumptions on the airborne fraction of total emissions (see Methods).

Emissions of road microplastics are concentrated in the eastern US, Northern Europe and large urbanized areas of Eastern China, Middle East and Latin America where vehicle densities are highest (Fig. 1, Extended Data Fig. 1). Annual total global TWP and BWP emissions were 2907 kt yr^{-1} and 175 kt yr^{-1}, respectively. For the PM2.5 and PM10 size fractions, TWP emissions were 29 kt yr^{-1} (12–75 kt yr^{-1}) and 288 kt yr^{-1} (113–826 kt yr^{-1}), respectively (Table 1). The highest emissions were calculated for Asia (excluding Russia) (PM2.5: 4.8–30 kt yr^{-1}, mean: 12 kt yr^{-1}; PM10: 85.0–167 kt yr^{-1}, mean: 113 kt yr^{-1}) and North America (PM2.5: 2.6–16 kt yr^{-1}, mean: 6.4 kt yr^{-1}; PM10: 46–90 kt yr^{-1}, mean: 64 kt yr^{-1}) (Fig. 1). The annual global emissions of BWP were 98.2 kt yr^{-1} (63.4–152 kt yr^{-1}) for PM2.5 and 146 kt yr^{-1} (85.8–248 kt yr^{-1}) for PM10 (Fig. 1, Extended Data Fig. 2). BWP emissions were very similar in Europe and North America for both PM2.5 and but higher in Asia (Table 1).

Atmospheric transport and deposition of road microplastics

Surface concentrations of TWPs range between a few ng m^{-3} and 20 ng m^{-3} for PM2.5 and up to 50 ng m^{-3} for PM10 (Video S 1). BWP surface concentrations reach 50 ng m^{-3} at maximum (Video S 1). The highest concentrations were calculated for eastern USA, Europe and Southeastern

Preprints (www.preprints.org) | NOT PEER-REVIEWED | Posted: 27 March 2020 doi:10.20944/preprints202003.0385.v1

Asia. These concentrations are below air quality limits (annual and daily mean: 10 μg m^{-3} and 25 μg m^{-3} for PM2.5, double for PM10[41]) but are comparable to typical black carbon (BC) concentrations in remote regions[42].

Annual deposition maps (Fig. 2) show that smaller microplastic particles (PM2.5) are dispersed more widely than larger ones (PM10) that are deposited mainly close to the hotspot emission regions (North America, Europe and Southeastern Asia) (Fig. 2). Of the annual global TWP PM2.5 emission of 29 kt yr^{-1} (12–75 kt yr^{-1}), about 1.7 kt yr^{-1} (0.60–4.8 kt yr^{-1}) were deposited over Europe, 4.3 kt yr^{-1} (1.5–12 kt yr^{-1}) over Asia, 3.3 kt yr^{-1} (1.1–9.6 kt yr^{-1}) in America, and much lower amounts in Africa and Oceania (<4% of the total deposited mass). Overall, 43% (4.3–34 kt yr^{-1}, mean: 12 kt yr^{-1}) of the total deposited mass of PM2.5 TWPs was deposited on land and 57% (5.3–48 kt yr^{-1}, mean: 16 kt yr^{-1}) in the ocean (Table 2). About 8.1 kt yr^{-1} (2.8–23 kt yr^{-1}) of PM2.5 TWPs were deposited on ice and snow surfaces (polar regions, mountains, etc.). Accordingly, annual total deposition of PM10 TWPs was 284 kt yr^{-1} (102–787 kt yr^{-1}) with ~65% (68.1–497 kt yr^{-1}, mean: 184 kt yr^{-1}) deposited on land. Around 28 kt yr^{-1} (10–76 kt yr^{-1}) of the TWPs were deposited on snow and ice. The vast majority (60%) was deposited in Europe, America, Russia and Asia (Table 2). Transport of TWPs to Antarctica was negligible.

Of the 97 kt yr^{-1} (59.2–162 kt yr^{-1}) annual total deposition of PM2.5 BWPs, 45 kt yr^{-1} (30–68 kt yr^{-1}) were deposited on land (46%) and 52 kt yr^{-1} (29–94 kt yr^{-1}) in the World Ocean (54%) (Table 2). About 14 kt yr^{-1} (11–18 kt yr^{-1}) were deposited in Asia, 12.9 kt yr^{-1} (8.6–19 kt yr^{-1}) in America, 6.1 kt yr^{-1} (4.7–7.9 kt yr^{-1}) over Europe, and 7.2 kt yr^{-1} (6.0–8.6 kt yr^{-1}) in Russia. A significant amount (~31%) of 30 kt yr^{-1} (20–45 kt yr^{-1}) was deposited on snow and ice surfaces. As regards to PM10 BWPs, half of the deposition (~53%) occurred in Asia, Europe and North America. About 72% (78.4–133 kt yr^{-1}, mean: 102 kt yr^{-1}) were deposited on the land and the rest in the ocean, and only 20 kt yr^{-1} (11–36 kt yr^{-1}) on snow and ice surfaces (~14% of global deposited mass). Similar to TWPs, transport to Antarctica was negligible. The slightly smaller relative deposition of BWPs over the ocean compared to TWPs in both particle sizes (Table 2) can be attributed to the higher particle density of BWPs (see Methods), which leads to more rapid deposition.

Concentrations of microplastics in snow-covered land and ice surfaces

TWP concentrations in the Arctic snow ranged between 1 and 10 ng kg^{-1} of snow for PM2.5 and between 4 and 80 ng kg^{-1} for PM10 (Fig. 3). Modelled concentrations of BWPs were 2–30 ng

Preprints (www.preprints.org) | NOT PEER-REVIEWED | Posted: 27 March 2020 doi:10.20944/preprints202003.0385.v1

kg^{-1} for PM2.5 and 2–70 ng kg^{-1} for PM10 (Fig. 3). For comparison, note that these values are almost three orders of magnitude lower than those of black carbon in Arctic snow[43,44]. It is seen that Northern Europe (e.g., Scandinavia), on one side, and North America on the other present higher snow concentrations than the Arctic. This is a combination of the proximity to source regions and the fact that the calculation was performed only for pixels with substantial snowfall as compared to total precipitation (see Video S 2). The largest Arctic snow concentrations were predicted on the sea-ice between Northern Greenland and Europe. This area receives road microplastics emitted both in North America and Europe (see Supplementary Video S 3 – Video S 5). Transport of microplastics into the Arctic occurs particularly in winter and spring (Fig. 3e-f) and is likely enhanced during positive phases of the North Atlantic Oscillation[45]. Another hot spot region, in terms of snow concentrations, is Northern Eurasia (Fig. 3). This region is affected by air transport from high-emission regions further south (Video S 3 – S 5).

The uncertainty of road microplastics deposition was calculated from 120 model ensemble members, each comprising different size distribution characteristics, different coefficients for in-cloud and below-cloud scavenging and variable airborne fraction with respect to total emissions (see Methods). The uncertainty was calculated as the geometric standard deviation of deposition resulting from all ensemble members (see Methods, Extended Data Fig. 3 and Extended Data Table 1).

The relative uncertainties in deposition both for PM2.5 and PM10 road microplastics are high, with a geometric standard deviation of up to 3. This is mainly due to the great uncertainty in the size distributions of emitted TWPs and BWPs, which controls the fraction of the total mass that can become airborne (PM10) and the removal properties within that fraction. Dannis[46] found that mean particle diameter of TWPs decreases while speed increases, which may contribute to the large differences in reported size distributions. In an effort to explain the size distribution, Cadle and Williams[47] suggested that the formation of sub-micron TWPs may be due to the thermal degradation of tyre polymer, with the larger particle mode being generated by mechanical abrasion. Deposition of PM2.5 road microplastics is more uncertain closer to the highest emitting continents (Northeastern USA, Southeastern China and Europe) and in tropical regions where precipitation is intense (Fig. 4a,c,e). On the contrary, the highest uncertainties for PM10 microplastic deposition occur in remote regions (Fig. 4b,d,e). This is related to the large sensitivity of long-range transport

Preprints (www.preprints.org) | NOT PEER-REVIEWED | Posted: 27 March 2020 doi:10.20944/preprints202003.0385.v1

efficiency to gravitational settling and below-cloud scavenging of larger particles, which is relatively more important for PM10 than PM2.5.

Discussion

To examine the susceptibility of different remote regions (e.g., oceans, Arctic, etc.) to TWP and BWP emissions, we computed the probability of road microplastics emitted globally to reach these remote regions via the atmosphere. We define the transport efficiency as the ratio between the mass of microplastics deposited in a remote area and the total mass of microplastics emitted globally. We calculate these efficiencies by masking several geographical regions (Table 3).

About 15% of the PM2.5 road microplastics were transported to the Atlantic Ocean (Table 3), whereas coarse particles were less efficiently deposited there (TWPs: 10%, BWPs: 11%). Due to the smaller size of PM2.5, their transport efficiency to the Pacific Ocean was even more strongly enhanced relative to PM10 deposition (Table 3). The South China Sea receives about 2% of airborne road microplastics, at maximum, a large amount considering its relatively small surface. This is due to the fact that Southeastern Asian emissions of microplastics tend to travel towards the South China Sea and the Western Pacific before they turn to the north, all the way to the Arctic (Video S 3 – S 5). The calculated transport of PM10 road microplastics shows a relatively high efficiency over Greenland (TWPs: 1.7%, BWPs: 2.3%) and over the Arctic Ocean (TWPs: 6.8%, BWPs: 4.3%). Negligible transport to the Southern Ocean and Antarctica was simulated.

A notable point here is the fact that in areas surrounded by microplastic emissions sources, PM10 particles are more efficiently deposited than PM2.5 particles. For instance, in the Alps, the Mediterranean, Baltic and South China Seas, transport efficiencies of coarse particles were up to twice of those of the fine particles. Short exposure to PM10 particles has been highlighted as a major cause of respiratory diseases (e.g., asthma), especially considering that such regions are heavily populated[41]. The opposite is the case in remote areas that are far from emission sources such as the Arctic and Greenland, where deposition of smaller particles is much more important (Table 3).

Another important receptor region of global microplastic emissions is the Arctic (Table 3). It is well known that aerosols can be transported efficiently to the Arctic, in particular during the Arctic Haze season in late winter and spring[48]. We find a transport efficiency of almost 3.6% for the Arctic (excluding Greenland) and a similar transport efficiency for Greenland. These transport patterns intensify the climatic risk of microplastic pollution with respect to their ability to decrease

Preprints (www.preprints.org) | NOT PEER-REVIEWED | Posted: 27 March 2020 doi:10.20944/preprints202003.0385.v1

the albedo in the Arctic and enhance snow and ice melting. In addition, road microplastics may concentrate in Arctic melt pools, with unknown ecological consequences. TWPs and BWPs constitute ~1.8% of total plastic production[14], hence the anticipated impact of all microplastics arriving to snow and ice surfaces might be greater.

One aspect that is missing from our simulations is potential re-suspension of road microplastics. Strong winds may re-mobilize deposited microplastic particles both from the land and the ocean surface, allowing secondary transport of these particles and thus enhancing efficiency of airborne transport to remote areas such as the Arctic, somewhat similar to the well-known grasshopper effect of persistent organic pollutants[49]. Another important aspect is the fact that emissions from non-road vehicles (tractors, mining trucks and equipment, construction and forestry machinery, and even military) have not been included in our emission inventories. While these vehicles are fewer, they work in difficult conditions, are heavier and carry heavy loads leading to enhanced tire and break wear.

There is a lack of measurement data that could be used to validate our results. However, Bergmann et al.[38] reported that the mean number concentration of plastic fibers detected in snow from Svalbard were 1.38±1.10 ml^{-1}, while in Bavaria they were 1.43±0.32 ml^{-1}. Also, 80% of all particles detected were <25 µm. According to Stylios[50], a microfibre is a fibre with less than 1 decitex (dtex) per filament with the most common types being from polyesters and polyamides (1 dtex = 1 mg per 10 m). Since the majority of the fibers was <25 µm size, these number concentrations can be converted to mass concentrations of 3.4±2.8 ng g^{-1} and 3.6±0.80 ng g^{-1} in Svalbard and Bavaria, respectively. Materic et al.[51] reported PET, PPC and PVC concentrations in Alpine snow of 5.6–23 ng g^{-1}, 11–16 ng g^{-1} and 6.9±0.2 ng g^{-1}, respectively. These concentrations are about 100 times higher than those estimated here for TWPs and BWPs in snow (see Fig. 3), which is likely realistic considering the larger usage of these polymers as compared to TWPs and BWPs.

We calculated that out of 102–787 kt (mean: 284 kt) of PM10 TWPs emitted, 34.4–290 kt (mean: 100 kt) were deposited in the World Ocean. In the most recent study on riverine transport from land to ocean, Wijnen et al.[52] reported a total annual global export of microplastics to the ocean of 47 kt, 80% (37.6 kt) of which was produced by macroplastic degradation, and 20% (9.4 kt) was from direct discharges of TWP and laundry fibres. The total annual releases of TWP in their model were assumed to be 426 kt (see Table 3 in Wijnen et al.[52]). If we assume that all

Preprints (www.preprints.org) | NOT PEER-REVIEWED | Posted: 27 March 2020 doi:10.20944/preprints202003.0385.v1

microplastics are transported from land to the World Ocean over time (wash-out and runoff processes) and scale the Wijnen et al.[52] TWP emissions to match ours (2907 kt, Fig. 1), we calculate that 64 kt of TWP may be washed out from the land in a year. This suggests that direct deposition of airborne road microplastics is likely the most important source for the ocean and marine biota.

Methods

TWP emission calculations based on a CO_2 ratio method. Top-down estimates of total annual tire wear emissions of 5,700 10,000 tonnes and 100,000 tonnes, respectively, have been reported for Norway[53], Sweden[54] and Germany[55], based on measurements of lifetime weight loss of returned tires. For the rest of the globe, we did not have access to such data. To obtain global emissions (Fig. 1), we assumed a constant ratio of TWP emissions to CO_2 emissions from the road transport sector (0.49 mg TWP/g CO_2), using CO_2 emissions from the CMIP6 (Coupled Model Intercomparison Project phase 6)[56] inventory (0.5°×0.5° resolution) for the year 2014. The TWP/CO_2 emission ratio is the average value of the ratios obtained for Norway, Sweden, and Germany, which were all very similar: 0.43, 0.50 and 0.55 mg TWP/g CO_2, respectively.

While the total TWP emission is relatively well constrained, the fraction of total TWP and BWP emissions that becomes airborne, assumed to be particles smaller than 10 µm (PM10), is highly uncertain. Values reported in the literature range from around 1% to 40%, while those for the PM2.5 fraction (particles smaller than 2.5 µm) are around 1%[21,28,30,36,57–60] (see also Table 6 in Grigoratos and Martini[61]). We examined how sensitive the calculated concentrations of TWP are with respect to this fraction. For that, we created five scenarios that assumed that 2.5%, 5%, 10%, 20% and 40% of the total TWP emitted are PM10 and 0.25%, 0.5%, 1%, 2% and 4% are PM2.5. We report TWP emissions as a range (geometric mean and geometric standard deviation) based on the derived emissions from the five ensemble members, each one with a different assumed fraction for the PM2.5 and PM10 mode.

TWP and BWP emission calculations with the GAINS model. The GAINS (Greenhouse gas – Air pollution Interactions and Synergies; http://gains.iiasa.ac.at) model[62] is an integrated assessment model where emissions of air pollutants and Kyoto gases are estimated for nearly two hundred regions globally considering key economic activities, environmental regulation policies, and regionally specific emission factors. For emissions of particulate matter (PM), GAINS

Preprints (www.preprints.org) | NOT PEER-REVIEWED | Posted: 27 March 2020 doi:10.20944/preprints202003.0385.v1

provides size speciated PM discriminating PM1, PM2.5, PM10, total PM, as well as carbonaceous particles (BC, OC); detailed description of the methodology can be found in Klimont et al.[63]. Emissions of non-exhaust PM in GAINS include TWPs, BWPs, and road abrasion and the calculation is based on region-specific data and estimates of distance driven (km/vehicle-type/year) and vehicle-type specific emission rates (mg/km). Distinguished vehicle-types for road transport include motorcycles, cars, light duty vehicles, buses, and heavy-duty vehicles. The estimates of distance driven for 2015 are derived using data on fuel use in road transport (from https://www.iea.org) supported by national data on vehicle numbers and assumptions of per-vehicle mileage travelled. Considering explicitly vehicle-type specific emission rates and respective activity data allows for better reflection of often significant regional differences in fleet structure, i.e., large number of motorcycles in South and South-East Asia and generally lower car ownership numbers in parts of the developing world. GAINS emissions are distributed globally (0.5°×0.5°) using road network data, assumptions about road-type vehicle density, and population data.

The vehicle-type specific TWP and BWP emission factors draw on review of several measurement papers (see Klimont et al.[64]) that were recently updated[63] using primarily van der Gon et al.[65], EEA[66] and Harrison et al.[36]. There are large uncertainties in emission factors including the PM size distribution. GAINS assumes that PM10 TWPs represent about 10% and PM2.5 about 1% of total TWPs, whereas PM10 BWPs is about 80% and PM2.5 is 40–50% of total BWPs independently on vehicle-type[64]. Here, we assumed that 2.5%, 5%, 10%, 20% and 40% of the total TWPs and 60%, 70%, 80%, 90% and 100% of the total BWPs is PM10 and then calculated the geometric mean and geometric standard deviation. Accordingly, 0.25%, 0.5%, 1%, 2% and 4% of total TWPs and 30%, 40%, 50%, 60% and 70% of total BWPs were assumed PM2.5, based on the range of values reported in the literature (see Table 3.96 and 3.97 in Klimont et al.[64] and references therein).

Preprints (www.preprints.org) | NOT PEER-REVIEWED | Posted: 27 March 2020 doi:10.20944/preprints202003.0385.v1

Atmospheric transport modelling of road microplastics. The gridded TWP emissions were adopted to the Lagrangian particle transport model FLEXPART (FLEXible PARTicle Dispersion Model) version 10.4[67–70]. The model was set to run in forward mode for year 2014 with a spin-up period of 1 month (December 2013). Boundary layer turbulent mixing and convection processes affecting particle transport in clouds are parameterised in the model[67,71]. The model was driven by 3-hourly 1°×1° operational analyses from the European Centre for Medium Range Weather Forecast (ECMWF), the spatial output resolution of concentration and deposition fields was set to 0.5°×0.5° in a global domain with a daily temporal resolution.

One of the most uncertain aspects of the TWP and BWP emissions is their size distribution. It depends on different properties of the tire, driving operation and composition and texture of the pavement[19]. Mathissen et al.[72], Sanders et al.[60] and Kumar et al.[59] reported that TWP and BWP can be even emitted as ultrafine particles due to a thermomechanical process that causes evaporation and re-condensation. A bimodal size distribution for TWP has been suggested with one maximum in the fine mode and another in the coarse mode[73–76]. On the contrary, an unimodal size distribution has been reported for BWP with maxima ranging between 1.0 and 6.0 μm[21,28,36,60,77] (Extended Data Fig. 3).

Model simulations were carried out for each of the above emission scenarios (five). However, since also the size distribution within the PM10 and PM2.5 modes is uncertain, we simulated particle transport for three different particle sizes in the PM2.5 (0.5, 1.0 and 2.1 μm) and five in the PM10 mode (0.5, 2.1, 3.2, 6.0 and 9.5 μm) and applied a range of different a posteriori weightings of these size classes (eight for each, Extended Data Fig. 3), thus enlarging our model ensemble to 40 members.

Yet another source of uncertainty is the efficiency with which particles are scavenged by precipitation. Plastics are generally hydrophobic and should therefore be rather inefficient cloud condensation nuclei (CCN)[78]. However, as known for black carbon, coatings may make the particles more hydrophilic with time in the atmosphere[40]. The efficiency of aerosols to serve as ice nuclei (IN) is also not well known. To bracket this type of uncertainty in our simulations, we accounted for three different in-cloud scavenging properties (low, medium, and high CCN/IN efficiency, Extended Data Table 1) in each of the aforementioned particle sizes, which lead to 120 model scenarios in total. We report simulated concentrations and deposition amounts as the

Preprints (www.preprints.org) | NOT PEER-REVIEWED | Posted: 27 March 2020 doi:10.20944/preprints202003.0385.v1

geometric mean values of the 120 ensemble members and quantify their uncertainty as their geometric standard deviation.

The simulations also accounted and below-cloud scavenging and dry deposition, assuming a particle density for TWPs of 1234 kg m^{-3}, which is in the middle of the densities of 945 kg m^{-3} for natural rubber and 1522 kg m^{-3} for synthetic rubber[79,80]. This density is within the reported range for microplastics (940-2400 kg m^{-3})[81]. For BWPs a higher density was assumed (2000 kg m^{-3}) considering that BWP may also contain metals[20]. These values were held constant for all ensemble members.

Statistics and uncertainty calculations in transport and deposition. We plot the probability density functions (PDF) for deposition of TWPs and BWPs that resulted from all the ensemble members of our sensitivity in Fig. S 2. In the present case, five ensemble members represented the uncertainty in the emissions, eight that in the size distribution (Extended Data Fig. 3) and three members that in the CCN/IN efficiency (Extended Data Table 1), which gives a total of 120 ensemble members for each size (PM2.5 and PM10). Fig. S 2 shows that deposition follows a lognormal distribution with a PDF that can be expressed as follows:

$$f(\chi, \mu_g, \sigma_g) = \frac{1}{\chi \sigma_g \sqrt{2\pi}} \exp\left(-\frac{(\ln x - \mu_g)^2}{2{\sigma_g}^2}\right)$$

where χ is the random variable, μ_g and σ_g are the mean and standard deviation of the distribution of lnχ. This relationship is true regardless of the base of the logarithmic or exponential function (see Limpert et al.[82]). Thus, the results can be expressed by the geometric mean (μ_g) and the uncertainty by the geometric standard deviation (σ_g) of χ, which are given below:

$$\mu_g = \sqrt[N]{A_1 A_2 \dots A_N} \text{ and } \sigma_g = \exp\left(\sqrt{\frac{\sum_{i=1}^{N} (\ln \frac{A_i}{\mu_g})^2}{N}}\right)$$

where $A_1, A_2, \dots, A_N$ are the results from each ensemble member and N the size of the ensemble (120 members for the PM2.5 and PM10 mode, respectively, for each of the TWP and BWP).

The geometric standard deviation is a dimensionless multiplicative factor, also called geometric SD factor[83]. We present resulting concentrations and deposition here with geometric SD factor in conjunction with geometric mean as "the range from “the geometric mean divided by the geometric SD factor” to “the geometric mean multiplied by the geometric SD factor”, rather add/subtract "geometric SD factor" to/from “geometric mean”[84].

Data availability

All primary sources (TWP and BWP emission data) are publicly available in https://doi.org/10.5061/dryad.qrfj6q5bx (temporary link: https://datadryad.org/stash/share/_dEIxj28-AHDSoIEPIRdufbljARA-NLyKYOs2n2CqqE) FLEXPART version 10.4 model is publicly available (see Pisso et al.[67]). Operational meteorological data that were used in FLEXPART version 10.4 model can be downloaded directly from the European Centre for Medium-Range Weather Forecasts (ECMWF, https://www.ecmwf.int) following their rules and regulations. All FLEXPART version 10.4 simulation results can be found in https://doi.org/10.5061/dryad.qrfj6q5bx (temporary link: https://datadryad.org/stash/share/_dEIxj28-AHDSoIEPIRdufbljARA-NLyKYOs2n2CqqE) or upon request to N.E. The same dataset also contains land-sea, ocean, continental and country masks that were used in the calculations of continental emissions, oceanic deposition and transport efficiencies, together with the ECMWF data of sea-ice area fraction, snow depth, snowfall and total precipitation that were used in the calculations of snow concentrations.

References

1. PlasticsEurope. Plastics – the facts 2018. (2018). Available at: https://www.plasticseurope.org/application/files/6315/4510/9658/Plastics_the_facts_2018_AF_web.pdf.
2. Blettler, M. C. M., Abrial, E., Khan, F. R., Sivri, N. & Espinola, L. A. Freshwater plastic pollution: Recognizing research biases and identifying knowledge gaps. *Water Res.* **143**, 416–424 (2018).
3. Haward, M. Plastic pollution of the world's seas and oceans as a contemporary challenge in ocean governance. *Nat. Commun.* **9**, 9–11 (2018).
4. Chae, Y. & An, Y. J. Current research trends on plastic pollution and ecological impacts on the soil ecosystem: A review. *Environ. Pollut.* **240**, 387–395 (2018).
5. Lebreton, L., Egger, M. & Slat, B. A global mass budget for positively buoyant macroplastic debris in the ocean. *Sci. Rep.* **9**, 1–10 (2019).
6. Peeken, I. *et al.* Arctic sea ice is an important temporal sink and means of transport for microplastic. *Nat. Commun.* **9**, (2018).
7. Wagner, S. & Reemtsma, T. Things we know and don't know about nanoplastic in the environment. *Nat. Nanotechnol.* **14**, 300–301 (2019).
8. Gewert, B., Plassmann, M. M. & Macleod, M. Pathways for degradation of plastic polymers floating in the marine environment. *Environ. Sci. Process. Impacts* **17**, 1513–1521 (2015).
9. Lamb, J. B. *et al.* Plastic waste associated with disease on coral reefs. *Science (80-.).* **359**, 460–462 (2018).
10. Wilcox, C., Puckridge, M., Schuyler, Q. A., Townsend, K. & Hardesty, B. D. A quantitative analysis linking sea turtle mortality and plastic debris ingestion. *Sci. Rep.* **8**,

1–11 (2018).
11. Harne, R. Studies on Plastic Bezoar Ingestion in Free Range Axis Deer in Summer. *J. Anim. Res.* 383–386 (2019). doi:10.30954/2277-940x.02.2019.25
12. Lehner, R., Weder, C., Petri-Fink, A. & Rothen-Rutishauser, B. Emergence of Nanoplastic in the Environment and Possible Impact on Human Health. *Environ. Sci. Technol.* **53**, 1748–1765 (2019).
13. Wright, S. L. & Kelly, F. J. Plastic and Human Health: A Micro Issue? *Environ. Sci. Technol.* **51**, 6634–6647 (2017).
14. Jan Kole, P., Löhr, A. J., Van Belleghem, F. G. A. J. & Ragas, A. M. J. Wear and tear of tyres: A stealthy source of microplastics in the environment. *Int. J. Environ. Res. Public Health* **14**, 1–4 (2017).
15. Penkała, M., Ogrodnik, P. & Rogula-Kozłowska, W. Particulate Matter from the Road Surface Abrasion as a Problem of Non-Exhaust Emission Control. *Environments* **5**, 9 (2018).
16. Sommer, F. *et al.* Tire abrasion as a major source of microplastics in the environment. *Aerosol Air Qual. Res.* **18**, 2014–2028 (2018).
17. Sundt, P., Syversen, F., Skogesal, O. & Schulze, P.-E. *Primary microplastic-pollution: Measures and reduction potentials in Norway*. *Miljodirektoratet.No* (2016).
18. Rogge, W. F., Hildemann, L. M., Mazurek, M. A., Cass, G. R. & Simoneit, B. R. T. Sources of Fine Organic Aerosol. 3. Road Dust, Tire Debris, and Organometallic Brake Lining Dust: Roads as Sources and Sinks. *Environ. Sci. Technol.* **27**, 1892–1904 (1993).
19. Wagner, S. *et al.* Tire wear particles in the aquatic environment - A review on generation, analysis, occurrence, fate and effects. *Water Res.* **139**, 83–100 (2018).
20. Grigoratos, T. & Martini, G. *Non-exhaust traffic related emissions. Brake and tyre wear PM*. (Publications Office of the European Union, 2014). doi:10.2790/21481
21. Kukutschová, J. *et al.* On airborne nano/micro-sized wear particles released from low-metallic automotive brakes. *Environ. Pollut.* **159**, 998–1006 (2011).
22. Chan, D. & Stachowiak, G. W. Review of automotive brake friction materials. *Proc. Inst. Mech. Eng. Part D J. Automob. Eng.* **218**, 953–966 (2004).
23. Thorpe, A. & Harrison, R. M. Sources and properties of non-exhaust particulate matter from road traffic: A review. *Sci. Total Environ.* **400**, 270–282 (2008).
24. Österle, W., Griepentrog, M., Gross, T. & Urban, I. Chemical and microstructural changes induced by friction and wear of brakes. *Wear* **250**–**251**, 1469–1476 (2001).
25. Kwak, J. H., Kim, H., Lee, J. & Lee, S. Characterization of non-exhaust coarse and fine particles from on-road driving and laboratory measurements. *Sci. Total Environ.* **458**–**460**, 273–282 (2013).
26. Mamakos, A., Arndt, M., Hesse, D. & Augsburg, K. Physical Characterization of Brake-Wear Particles in a PM Dilution Tunnel. (2019).
27. Olofsson, U. & Olander, L. On the identification of wear modes and transitions using airborne wear particles. *Tribol. Int.* **59**, 104–113 (2013).
28. Mosleh, M., Blau, P. J. & Dumitrescu, D. Characteristics and morphology of wear particles from laboratory testing of disk brake materials. *Wear* **256**, 1128–1134 (2004).
29. Jan Kole, P., Löhr, A. J., Van Belleghem, F. G. A. J. & Ragas, A. M. J. Wear and tear of tyres: A stealthy source of microplastics in the environment. *Int. J. Environ. Res. Public Health* **14**, (2017).
30. Wik, A. & Dave, G. Occurrence and effects of tire wear particles in the environment - A critical review and an initial risk assessment. *Environ. Pollut.* **157**, 1–11 (2009).

31. Reynolds, C. & Ryan, P. G. Micro-plastic ingestion by waterbirds from contaminated wetlands in South Africa. *Mar. Pollut. Bull.* **126**, 330–333 (2018).
32. Dorsey, T. F. *et al.* Correlations of asthma mortality with traffic-related factors: Use of catalytic converters and radial tires. *J. Occup. Environ. Med.* **48**, 1321–1327 (2006).
33. Ashton, K., Holmes, L. & Turner, A. Association of metals with plastic production pellets in the marine environment. *Mar. Pollut. Bull.* **60**, 2050–2055 (2010).
34. Höök, M. & Tang, X. Depletion of fossil fuels and anthropogenic climate change-A review. *Energy Policy* **52**, 797–809 (2013).
35. Royer, S.-J., Ferron, S., Wilson, S. T. & Karl, D. M. Production of methane and ethylene from plastic in the environment. *PLoS One* **13**, e0200574 (2018).
36. Harrison, R. M., Jones, A. M., Gietl, J., Yin, J. & Green, D. C. Estimation of the contributions of brake dust, tire wear, and resuspension to nonexhaust traffic particles derived from atmospheric measurements. *Environ. Sci. Technol.* **46**, 6523–6529 (2012).
37. Allen, S. *et al.* Atmospheric transport and deposition of microplastics in a remote mountain catchment. *Nat. Geosci.* **12**, 339–344 (2019).
38. Bergmann, M. *et al.* White and wonderful? Microplastics prevail in snow from the Alps to the Arctic. *Sci. Adv.* **5**, 1–11 (2019).
39. Dris, R., Gasperi, J., Saad, M., Mirande, C. & Tassin, B. Synthetic fibers in atmospheric fallout: A source of microplastics in the environment? *Mar. Pollut. Bull.* **104**, 290–293 (2016).
40. Bond, T. C. *et al.* Bounding the role of black carbon in the climate system: A scientific assessment. *J. Geophys. Res. Atmos.* **118**, 5380–5552 (2013).
41. World Health Organization (WHO). WHO Air quality guidelines for particulate matter, ozone, nitrogen dioxide and sulfur dioxide. Global update 2005. *WHO/SDE/PHE/OEH/06.02* 1–21 (2005). Available at: https://apps.who.int/iris/bitstream/handle/10665/69477/WHO_SDE_PHE_OEH_06.02_eng.pdf?sequence=1.
42. Eckhardt, S. *et al.* Current model capabilities for simulating black carbon and sulfate concentrations in the Arctic atmosphere: A multi-model evaluation using a comprehensive measurement data set. *Atmos. Chem. Phys.* **15**, 9413–9433 (2015).
43. Doherty, S. J., Warren, S. G., Grenfell, T. C., Clarke, A. D. & Brandt, R. E. Light-absorbing impurities in Arctic snow. *Atmos. Chem. Phys.* **10**, 11647–11680 (2010).
44. Evangeliou, N. *et al.* Origin of elemental carbon in snow from Western Siberia and northwestern European Russia during winter – spring. *Atmos. Chem. Phys.* **18**, 963–977 (2018).
45. Eckhardt, S. *et al.* The North Atlantic Oscillation controls air pollution transport to the Arctic. *Atmos. Chem. Phys. Atmos. Chem. Phys.* **3**, 1769–1778 (2003).
46. Dannis, M. L. Rubber dust from the normal wear of tires. *Rubber Chemistry and Technology* **47**, 1011–1037 (1974).
47. Cadle, S. H. & Williams, R. L. Gas and particle emissions from automobile tires in laboratory and field studies. *J. Air Pollut. Control Assoc.* **28**, 502–507 (1978).
48. Stohl, A. Characteristics of atmospheric transport into the Arctic troposphere. *J. Geophys. Res. Atmos.* **111**, 1–17 (2006).
49. Simonich, S. L. & Hites, R. A. Global distribution of persistent organochlorine compounds. *Science (80-.).* **269**, 1851–1854 (1995).
50. Stylios, G. K. The appearance of seams in non-iron shirts. *Join. Text. Princ. Appl.* 467–477 (2013). doi:10.1533/9780857093967.4.467

51. Materić, D. *et al.* Micro- and Nanoplastics in Alpine Snow: A New Method for Chemical Identification and (Semi)Quantification in the Nanogram Range. *Environ. Sci. Technol.* (2020). doi:10.1021/acs.est.9b07540
52. van Wijnen, J., Ragas, A. M. J. & Kroeze, C. Modelling global river export of microplastics to the marine environment: Sources and future trends. *Sci. Total Environ.* **673**, 392–401 (2019).
53. Sundt, P. et al. Sundt, Schultze, Syversen - 2014 - Sources of microplastic- pollution to the marine environment Project report.pdf. (2014). doi:M-321|2015
54. Norén, F. & Naustvoll, L. J. Survey of microscopic anthropogenic particles in Skagerrak. Pilot study October-November 2010 . 19 (2010).
55. Essel, R., Engel, L., Carus, M. & Ahrens, R. H. *Quellen für Mikroplastik mit Relevanz für den Meeresschutz in Deutschland*. **8**, (2015).
56. Simpkins, G. Progress in climate modelling. *Nat. Clim. Chang.* **7**, 684–685 (2017).
57. Panko, J. M., Chu, J., Kreider, M. L. & Unice, K. M. Measurement of airborne concentrations of tire and road wear particles in urban and rural areas of France, Japan, and the United States. *Atmos. Environ.* **72**, 192–199 (2013).
58. Garg, B. D. *et al.* Brake wear particulate matter emissions. *Environ. Sci. Technol.* **34**, 4463–4469 (2000).
59. Kumar, P., Pirjola, L., Ketzel, M. & Harrison, R. M. Nanoparticle emissions from 11 non-vehicle exhaust sources - A review. *Atmos. Environ.* **67**, 252–277 (2013).
60. Sanders, P. G., Xu, N., Dalka, T. M. & Maricq, M. M. Airborne brake wear debris: Size distributions, composition, and a comparison of dynamometer and vehicle tests. *Environ. Sci. Technol.* **37**, 4060–4069 (2003).
61. Grigoratos, T. & Martini, G. Brake wear particle emissions: a review. *Environ. Sci. Pollut. Res.* **22**, 2491–2504 (2015).
62. Amann, M. *et al.* Cost-effective control of air quality and greenhouse gases in Europe: Modeling and policy applications. *Environ. Model. Softw.* **26**, 1489–1501 (2011).
63. Klimont, Z. *et al.* Global anthropogenic emissions of particulate matter including black carbon. *Atmos. Chem. Phys.* **17**, 8681–8723 (2017).
64. Klimont, Z. *et al.* Modelling Particulate Emissions in Europe. *IIASA, Interim Rep.* **IR-02-076**, (2002).
65. Denier van der Gon, H. A. C. *et al.* The PolicyRelevance of WearEmissions fromRoad Transport,Nowand in the Future-An InternationalWorkshop Report and Consensus Statement. *J. Air Waste Manag. Assoc.* **63**, 136–149 (2013).
66. Eea. EMEP/EEA air pollutant emission inventory guidebook 2013: Technical guidance to prepare national emission inventories. *EEA Tech. Rep.* 23 (2013). doi:10.2800/92722
67. Pisso, I. *et al.* The Lagrangian particle dispersion model FLEXPART version 10.4. *Geosci. Model Dev.* **12**, 4955–4997 (2019).
68. Fang, X. *et al.* Sulfur hexafluoride (SF6) emissions in East Asia determined by inverse modeling. *Atmos. Chem. Phys.* **14**, 4779–4791 (2014).
69. Thompson, R. L. *et al.* Methane emissions in East Asia for 2000-2011 estimated using an atmospheric Bayesian inversion. *J. Geophys. Res. Atmos.* **120**, 4352–4369 (2015).
70. Mühle, J. *et al.* Perfluorocyclobutane (PFC-318, <i>c</i>-C4F8) in the global atmosphere. *Atmos. Chem. Phys.* **19**, (2019).
71. Forster, C., Stohl, A. & Seibert, P. Parameterization of convective transport in a Lagrangian particle dispersion model and its evaluation. *J. Appl. Meteorol. Climatol.* **46**, 403–422 (2007).

72. Mathissen, M., Scheer, V., Vogt, R. & Benter, T. Investigation on the potential generation of ultrafine particles from the tire-road interface. *Atmos. Environ.* **45**, 6172–6179 (2011).
73. Fukahori, Y. & Yamazaki, H. Mechanism of rubber abrasion. Part I: Abrasion pattern formation in natural rubber vulcanizate. *Wear* **171**, 195–202 (1994).
74. Gustafsson, M. *et al.* Properties and toxicological effects of particles from the interaction between tyres, road pavement and winter traction material. *Sci. Total Environ.* **393**, 226–240 (2008).
75. Wang, Q., Zhang, Q., Wu, Y. & Wang, X. C. Physicochemical conditions and properties of particles in urban runoff and rivers: Implications for runoff pollution. *Chemosphere* **173**, 318–325 (2017).
76. Kreider, M. L., Panko, J. M., McAtee, B. L., Sweet, L. I. & Finley, B. L. Physical and chemical characterization of tire-related particles: Comparison of particles generated using different methodologies. *Sci. Total Environ.* **408**, 652–659 (2010).
77. Iijima, A. *et al.* Particle size and composition distribution analysis of automotive brake abrasion dusts for the evaluation of antimony sources of airborne particulate matter. *Atmos. Environ.* **41**, 4908–4919 (2007).
78. Di Mundo, R., Petrella, A. & Notarnicola, M. Surface and bulk hydrophobic cement composites by tyre rubber addition. *Constr. Build. Mater.* **172**, 176–184 (2018).
79. Walker, R. The mass of 300 different 'dry' materials. (2019). Available at: https://www.simetric.co.uk/si_materials.htm. (Accessed: 14th October 2019)
80. User Guidelines for Waste and Byproduct Materials in Pavement Construction. *Federal Highway Administration Research and Technology* (2019). Available at: https://www.fhwa.dot.gov/publications/research/infrastructure/structures/97148/st1.cfm. (Accessed: 14th October 2019)
81. Unice, K. M. *et al.* Characterizing export of land-based microplastics to the estuary - Part I: Application of integrated geospatial microplastic transport models to assess tire and road wear particles in the Seine watershed. *Sci. Total Environ.* **646**, 1639–1649 (2019).
82. Limpert, E., Stahel, W. A. & Abbt, M. Log-normal Distributions across the Sciences: Keys and Clues. *Bioscience* **51**, 341–352 (2001).
83. Kirkwood, T. B. L. Geometric standard deviation - reply to bohidar. *Drug Dev. Ind. Pharm.* **19**, 395–396 (1993).
84. Kirkwood, T. B. L. Geometric Means and Measures of Dispersion. *Biometrics* **35**, 908–909 (1979).
85. Grythe, H. *et al.* A new aerosol wet removal scheme for the Lagrangian particle model FLEXPARTv10. *Geosci. Model Dev.* **10**, 1447–1466 (2017).

Acknowledgements

This work was supported by COMBAT (Quantification of Global Ammonia Sources constrained by a Bayesian Inversion Technique) funded by ROMFORSK – Program for romforskning of the Research Council of Norway (Project ID: 275407), website: **https://www.forskningsradet.no/prosjektbanken/#/project/NFR/275407**.

Author information

Affiliations

Norwegian Institute for Air Research (NILU), Instituttveien 18, 2007 Kjeller, Norway.
N. Evangeliou, H. Grythe, S. Eckhardt, S. Lopez-Aparicio & A. Stohl

International Institute for Applied Systems Analysis (IIASA), 2361 Laxenburg, Austria.
Z. Klimont & C. Heyes

Department of Meteorology and Geophysics, University of Vienna, UZA II, Althanstraße 14, 1090 Vienna, Austria
A. Stohl

Contributions

N.E. performed the simulations, analyses, wrote and coordinated the paper. H.G. and S.L.A. made the calculations of TWP emissions with the CO_2 ratio method, Z.K. and C.H. calculated TWP and BWP emissions with the GAINS model, S.E. helped in the FLEXPART version 10.4 simulations and A.S. wrote and commented on the manuscript. All authors contributed in the final version.

Corresponding author

Correspondence and request for materials should be addressed to N. Evangeliou (Nikolaos.Evangeliou@nilu.no).

Ethics declarations

Competing interests

The authors declare no competing financial interests.

Additional information

Peer review information Nature thanks the anonymous, reviewer(s) for their contribution to the peer review of this work.
Supplementary information is available for this paper at **+++.**
Reprints and permissions information is available at +++.

Preprints (www.preprints.org) | NOT PEER-REVIEWED | Posted: 27 March 2020 doi:10.20944/preprints202003.0385.v1

Extended data figures and tables

Extended Data Table 1. Different scavenging parameters of below–cloud and in–cloud scavenging used in FLEXPART version 10.4 for the ensemble model simulations of microplastics. $\boldsymbol{A}$ and $\boldsymbol{B}$ are rain and snow collection efficiencies for below-cloud scavenging, $\boldsymbol{A_i}$ is the cloud condensation nuclei (CCN) efficiency and $\boldsymbol{B_i}$ the ice nuclei (IN) efficiency that are used in in-cloud scavenging following Grythe et al.[85]. These values were used in the ensemble of 120 members (see **Methods**) with different assumption for the airborne fraction (five for each of the PM2.5 and PM10 fractions, **Methods**), particle size distribution (eight for each of the PM2.5 and PM10 fractions, **Extended Data Fig. 3**) and CCN/IN efficiency (three different sets of scavenging coefficients per fraction, **Extended Data Table 1**).

	$\boldsymbol{A}$	$\boldsymbol{B}$	$\boldsymbol{A_i}$	$\boldsymbol{B_i}$
Low efficiency	1	1	0.001	0.01
Medium efficiency	1	1	0.05	0.15
High efficiency	1	1	0.5	0.8

Preprints (www.preprints.org) | NOT PEER-REVIEWED | Posted: 27 March 2020 doi:10.20944/preprints202003.0385.v1

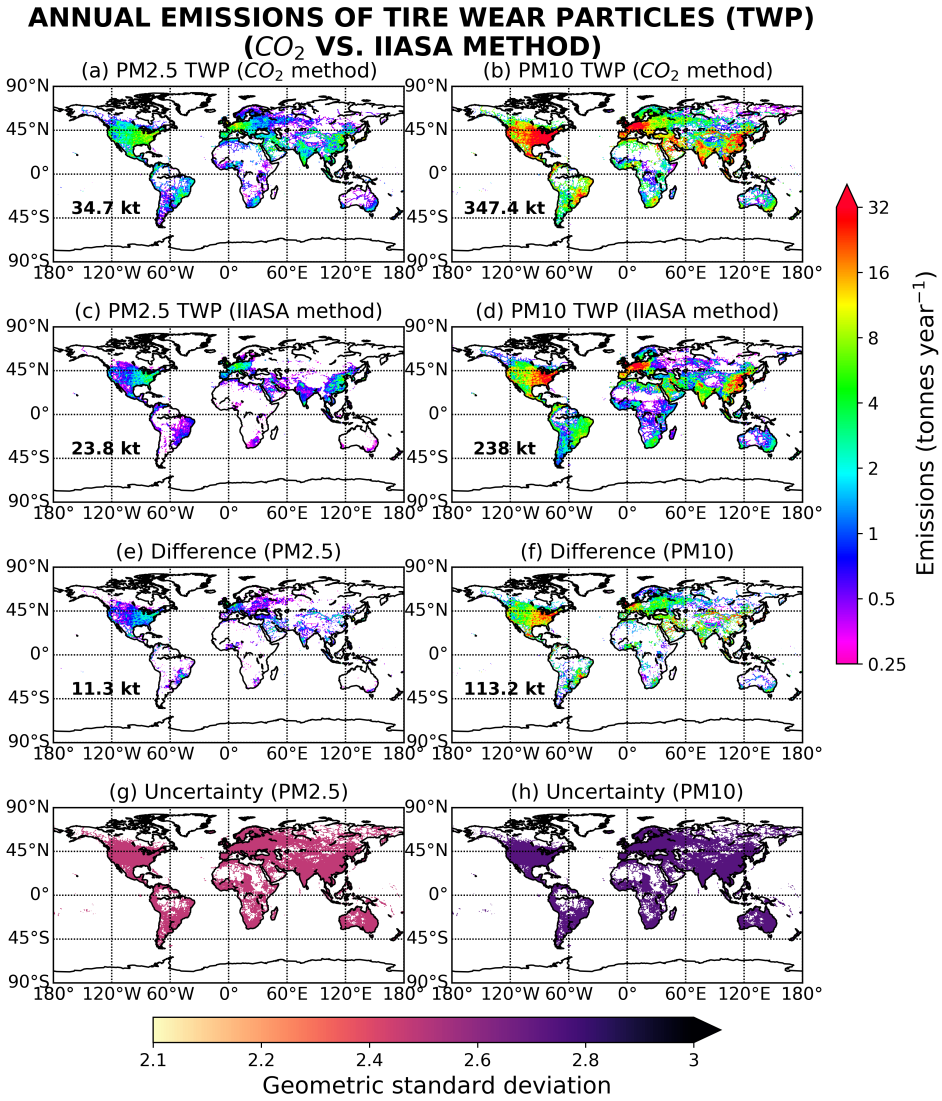

Extended Data Fig. 1. Annual emissions of TWPs with the CO_2 ratio method (panels a and b) and using the GAINS model (panels c and d) for PM2.5 and PM10 particles, respectively (**Fig. 1** and **Methods**). Emissions were calculated as the geometric mean of the five scenarios for the airborne fraction of total TWPs, assuming 2.5%, 5%, 10%, 20% and 40% of the total TWP are emitted as PM10 and 0.25%, 0.5%, 1%, 2% and 4% as PM2.5 following a log-normal distribution (**Fig. S 2**). Difference in emissions using the two different methodologies are presented in panels e and f. Uncertainties for the PM2.5 and PM10 TWP emissions (panels g and h) were calculated as the geometric standard deviation of the five assumed different airborne fractions per size mode (PM2.5 and PM10) with respect to total TWP emissions (see **Methods**). Bold numbers at the lower left side of panels a–d represent total annual emissions of TWPs, whereas bold numbers at the lower left side of panels e and f are the respective annual differences in the emissions of TWPs from the two methodologies used.

Preprints (www.preprints.org) | NOT PEER-REVIEWED | Posted: 27 March 2020 doi:10.20944/preprints202003.0385.v1

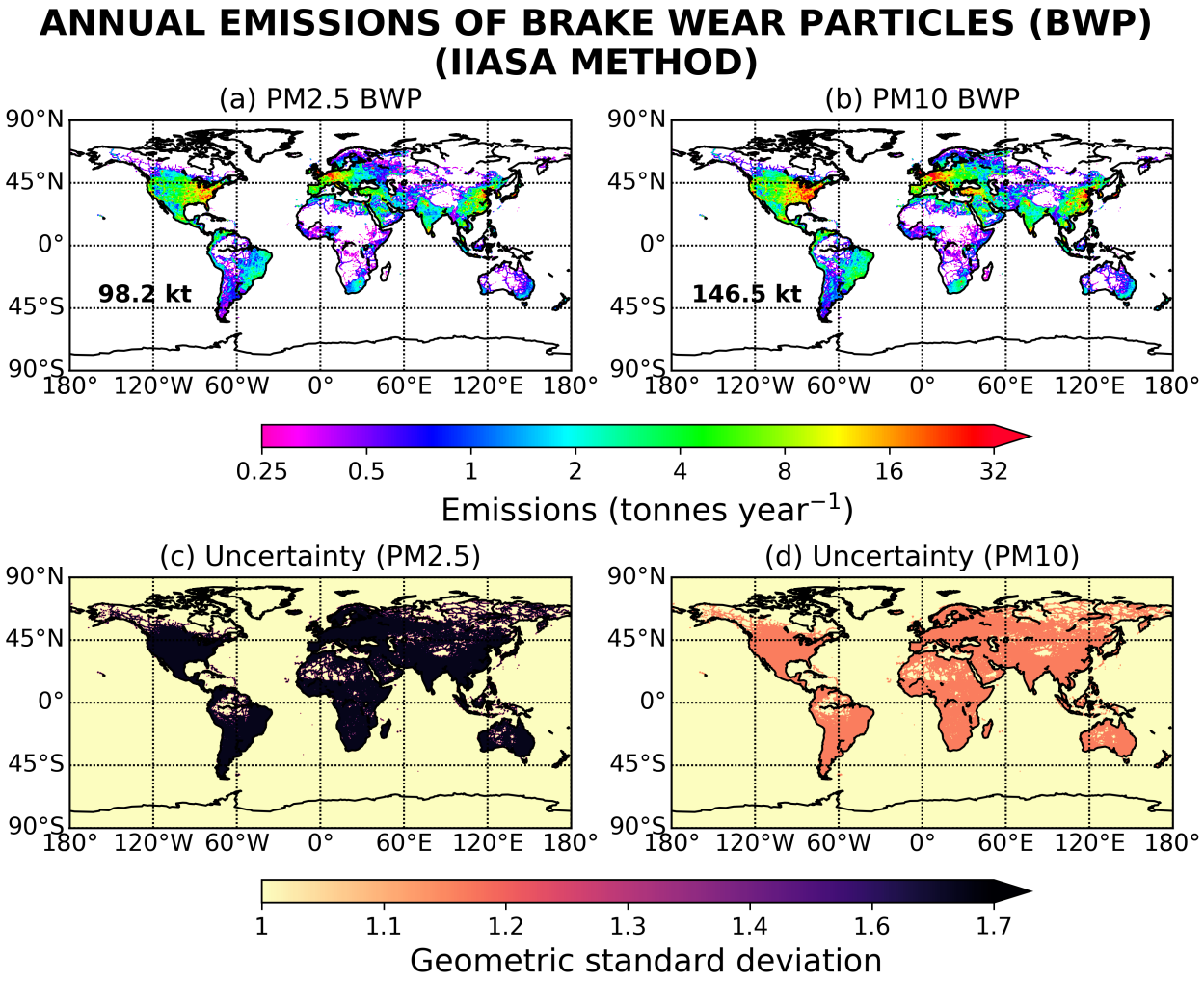

Extended Data Fig. 2. Annual emissions of BWPs from the GAINS model (panels a and b) for PM2.5 and PM10, respectively. The emissions are the geometric mean of five different assumptions on the airborne fraction for each size bin (30%, 40%, 50%, 60% and 70% of total BWPs were assumed to be PM2.5 and 60%, 70%, 80%, 90% and 100% of the total BWPs to be PM10) following a log-normal distribution (**Fig. S 2**). The estimated associated uncertainty (panels c and d) is expressed with the geometric standard deviation of the aforementioned scenarios (see **Methods**). Bold numbers at the lower left side of panels a and b represent total annual emissions of BWPs.

Preprints (www.preprints.org) | NOT PEER-REVIEWED | Posted: 27 March 2020 doi:10.20944/preprints202003.0385.v1

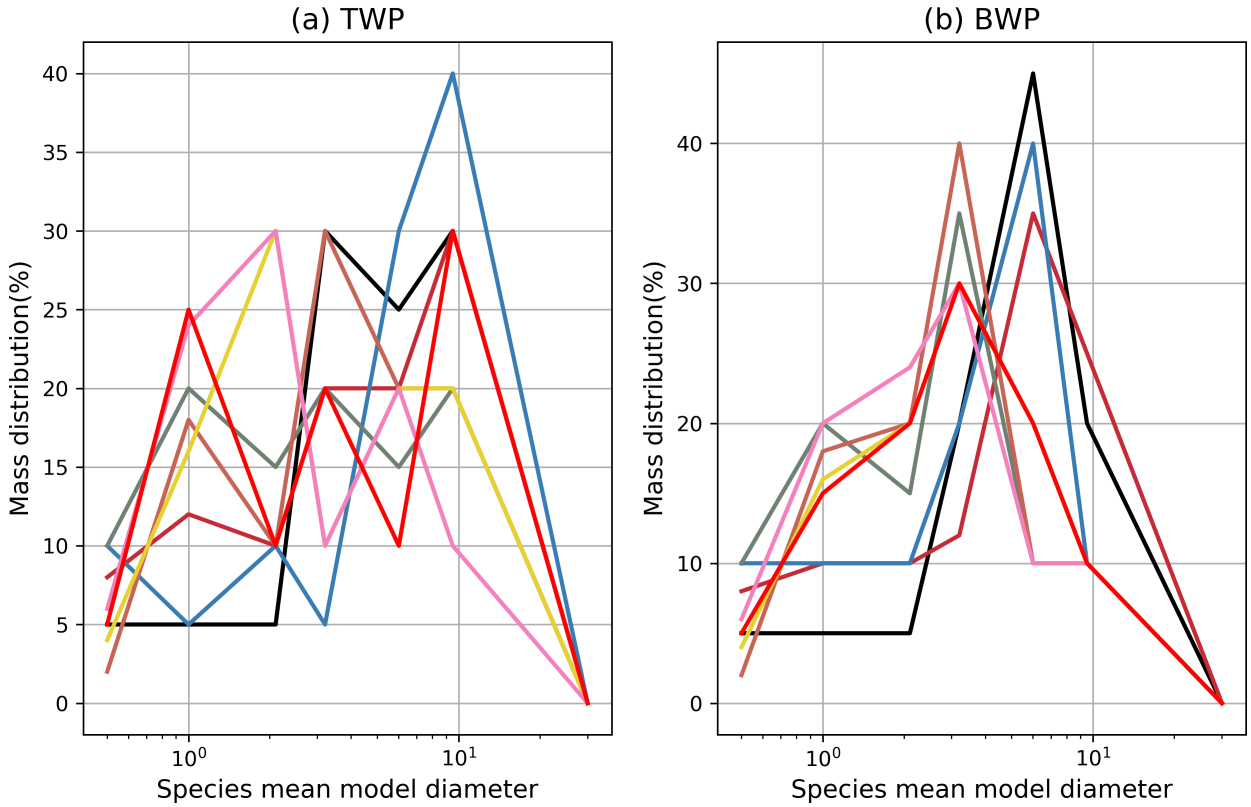

Extended Data Fig. 3. Size distribution used in the simulations of road microplastics (TWPs and BWPs) presenting a set of different a posteriori weightings for different size classes (eight for each of the TWP and BWP simulations). Three size classes were used for PM2.5 (0.5, 1.0 and 2.1 µm) and five for the PM10 mode (0.5, 2.1, 3.2, 6.0 and 9.5 µm). Note the bimodal (two peaks)[73–76] size distribution of TWPs with one maximum close to the fine mode and another in the coarse mode and the unimodal (single peak)[21,28,36,60,77] distribution of BWPs with maximum in the fine or coarse mode.

Preprints (www.preprints.org) | NOT PEER-REVIEWED | Posted: 27 March 2020 doi:10.20944/preprints202003.0385.v1

TABLE LEGENDS

Table 1. Annual continental emissions (in kt) of road microplastics (TWPs and BWPs) in PM2.5 and PM10 size modes averaged for the two different methodologies used (CO_2 ratio and GAINS model emissions). Corresponding ranges are variations of continental geometric standard deviations from geometric means (presented in parenthesis) following a log-normal distribution (see **Methods**, **Fig. S 2**). The airborne PM10 fraction was assumed to be 2.5%, 5%, 10%, 20% and 40% of the total TWP emissions, while the PM2.5 was assumed to be 0.25%, 0.5%, 1%, 2% and 4% of the total TWP emissions. For BWPs, it was assumed that 30%, 40%, 50%, 60% and 70% of total BWPs are PM2.5 and 60%, 70%, 80%, 90% and 100% of the total BWPs are PM10. Note that Russia has been excluded from both Europe and Asia and is listed separately, while America has been divided into three parts (north, central, south).

	Europe	**Asia**	**Russia**	**North America**	**Central America**	**South America**	**Africa**	**Oceania**	**Total**
PM2.5 TWP	2.3–15 (5.8)	4.8–30 (12)	0.26–1.6 (0.64)	2.6–16 (6.4)	0.32–2.0 (0.80)	0.8–5.0 (2.0)	0.56–3.5 (1.4)	0.19–1.2 (0.48)	**12–75 (29)**
PM10 TWP	42–82 (58)	85.0–167 (113)	4.6–9.0 (6.4)	46–90 (64)	5.7–11 (8.0)	14–28 (20)	10–20 (14)	3.4–6.8 (4.8)	**113–826 (288)**
PM2.5 BWP	13–32 (21)	26–62 (40)	2.5–6.0 (3.9)	11–26 (17)	1.7–4.0 (2.6)	4.4–10 (6.8)	3.4–8.1 (5.2)	0.97–2.3 (1.5)	**63.4–152 (98.2)**
PM10 BWP	28–37 (32)	50–67 (58)	6.9–9.1 (7.9)	22–29 (25)	3.2–4.2 (3.7)	8.4–11 (9.7)	6.5–8.6 (7.5)	1.9–2.5 (2.2)	**85.8–248 (146)**

 doi:10.20944/preprints202003.0385.v1

Table 2. Annual global (wet and dry) deposition (in kt) of road microplastics (TWPs and BWPs) in PM2.5 and PM10 size bins estimated with FLEXPART version 10.4 model. TWP deposition (average values are presented in parentheses) is the geometric mean of the two simulations with emissions calculated with the CO_2 ratio method and the GAINS model (IIASA) each including 120 ensemble members with different assumption for the airborne fraction (five for each of the PM2.5 and PM10 fractions, **Methods**), particle size distribution (eight for each of the PM2.5 and PM10 fractions, **Extended Data Fig. 3**) and CCN/IN efficiency (three different sets of scavenging coefficients per fraction, **Extended Data Table 1**). BWP deposition was calculated in the same way (120 ensemble members) but only using emissions from the GAINS model. Uncertainties of TWP and BWP deposition are expressed with the geometric standard deviation taking into account all the simulations (120). The results are given in ranges based on the variation of the geometric standard deviation from the geometric mean (**Methods**).

	Europe	**Asia**	**Russia**	**North America**	**Central America**	**South America**	**Africa**	**Oceania**	**Antarctica**	**Land**	**Ocean**	**Snow/Ice**	**Total**
PM2.5 TWP	0.60–4.8 (1.7)	1.5–12 (4.3)	0.53–3.6 (1.5)	0.76–6.4 (2.2)	0.11–0.90 (0.32)	0.27–2.3 (0.80)	0.38–3.2 (1.1)	0.03–0.2 (0.08)	– (0)	4.3–34 (12)	5.3–48 (16)	2.8–23 (8.1)	9.6–82 (**28**)
PM10 TWP	11–84 (31)	24.7–180 (66.8)	4.4–32 (12)	15.5–113 (41.9)	1.9–14 (5.1)	5.1–37 (14)	4.4–32 (12)	0.70–5.1 (1.9)	– (0)	68.1–497 (184)	34.4–290 (100)	10–76 (28)	102–787 (**284**)
PM2.5 BWP	4.7–7.9 (6.1)	11–18 (14)	6.0–8.6 (7.2)	5.9–13 (8.8)	0.80–1.8 (1.2)	1.9–4.4 (2.9)	2.6–6.7 (4.2)	0.18–0.40 (0.27)	– (0)	30–68 (45)	29–94 (52)	20–45 (30)	59.2–162 (**97**)
PM10 BWP	13–22 (17)	27–46 (35)	6.7–11 (8.7)	18–30 (23)	1.8–3.0 (2.3)	5.6–9.5 (7.3)	5.4–9.1 (7.0)	0.92–1.6 (1.2)	– (0)	78.4–133 (102)	23–68 (40)	11–36 (20)	101–201 (**142**)

 doi:10.20944/preprints202003.0385.v1

Table 3. Transport efficiencies (%) of road microplastics over remote areas. Transport efficiency is defined as the ratio between the mass of microplastics deposited in a remote region divided by the total mass of microplastics emitted globally (Error! Reference source not found.). Results are given as geometric means (presented in parentheses) that are based on simulations from different scenarios for the airborne fraction in the emissions (five for each of the PM2.5 and PM10 fractions, **Methods**), different particle size distribution for transport (eight for each of the PM2.5 and PM10 fractions, **Extended Data Fig. 3**) and different CCN/IN efficiency for deposition (three different sets of scavenging coefficients per fraction, **Extended Data Table 1**). Uncertainties have been calculated as the geometric standard deviation of all simulations (120) using the aforementioned assumptions and they are expressed as ranges of the geometric standard deviation from the geometric mean (**Methods**).

	Arctic	**Alps**	**Himalayas**	**Greenland**	**Atlantic Ocean**	**Pacific Ocean**	**Indian Ocean**	**Southern Ocean**	**Arctic Ocean**	**Mediterranean Sea**	**Baltic Sea**	**South China Sea**
PM2.5 TWP	1.2–10 (3.5)	0.11–0.84 (0.30)	0.048–0.45 (0.15)	1.2–9.5 (3.4)	5.4–42 (15)	6.3–57 (19)	1.9–15 (5.3)	0.43–3.4 (1.2)	5.0–39 (14)	0.080–0.72 (0.24)	0.018–0.14 (0.051)	0.19–1.4 (0.52)
PM10 TWP	0.46–3.1 (1.2)	0.22–1.4 (0.56)	0.046–0.31 (0.12)	0.65–4.4 (1.7)	3.7–27 (10)	4.3–34 (12)	1.3–11 (3.9)	0.52–3.8 (1.4)	2.4–19 (6.8)	0.16–1.1 (0.42)	0.024–0.15 (0.061)	0.32–2.0 (0.78)
PM2.5 BWP	2.4–5.4 (3.6)	0.22–0.49 (0.33)	0.078–0.25 (0.14)	2.3–5.1 (3.4)	10–22 (15)	9.1–36 (18)	3.2–8.1 (5.1)	0.60–2.0 (1.1)	10–20 (14)	0.13–0.48 (0.25)	0.041–0.069 (0.053)	0.41–0.59 (0.49)
PM10 BWP	1.0–1.7 (1.3)	0.50–0.85 (0.65)	0.078–0.15 (0.11)	1.4–3.7 (2.3)	6.9–18 (11)	5.2–23 (11)	1.2–5.1 (3.2)	0.27–0.94 (0.52)	2.7–6.7 (4.3)	0.35–0.58 (0.45)	0.055–0.092 (0.071)	0.65–1.3 (0.91)

 doi:10.20944/preprints202003.0385.v1

Preprints (www.preprints.org) | NOT PEER-REVIEWED | Posted: 27 March 2020 doi:10.20944/preprints202003.0385.v1

FIGURE LEGENDS

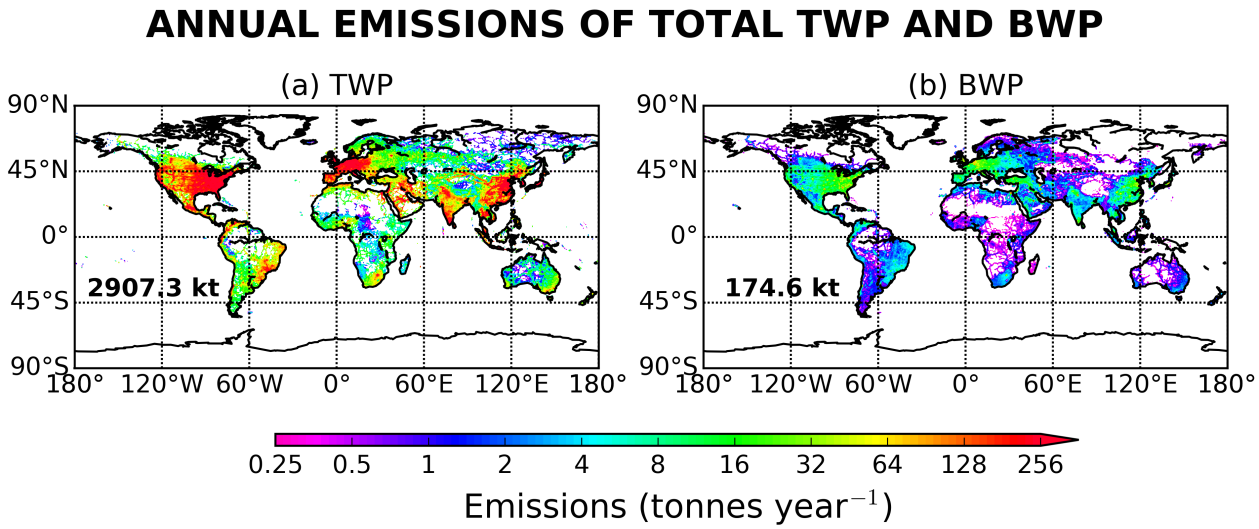

Fig. 1. Global annual emissions of total road microplastics (TWPs in panel a and BWPs in panel b). TWP emissions are the average of the calculated emissions using the CO_2 ratio method and the GAINS model (see **Extended Data Fig. 1** and **Extended Data Fig. 2**). Bold numbers at the left bottom of each panel represent the annual emissions of total TWPs and BWPs from road vehicles for 2014, which were estimated to be 2907 kt and 174.6 kt, respectively.

Preprints (www.preprints.org) | NOT PEER-REVIEWED | Posted: 27 March 2020 doi:10.20944/preprints202003.0385.v1

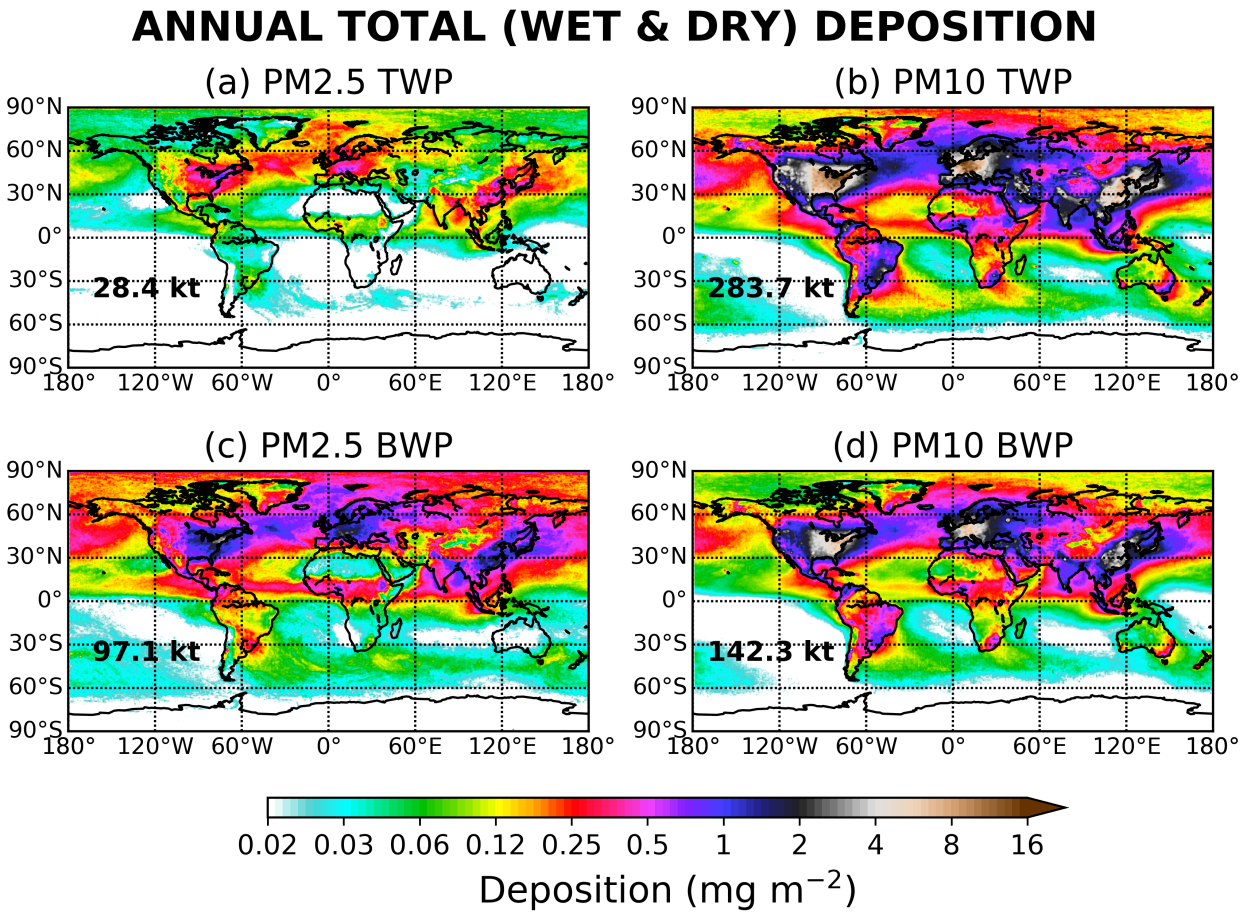

Fig. 2. Annual total (wet and dry) deposition of TWPs and BWPs in PM2.5 and PM10 size classes, respectively. The projected deposition has been calculated as the geometric mean of all simulations using TWP emissions estimated using the CO_2 ratio method and the GAINS model and using BWP emissions calculated from the GAINS model, respectively. The simulations comprise 120 ensemble members with different assumption for the airborne fraction (five for each of the PM2.5 and PM10 fractions, **Methods**), particle size distribution (eight for each of the PM2.5 and PM10 fractions, **Extended Data Fig. 3**) and CCN/IN efficiency (three different sets of scavenging coefficients per fraction, **Extended Data Table 1**) following a log-normal distribution (see **Methods** and **Fig. S 2**). Bold numbers at the left bottom of each panel represent the annual total deposition of TWPs and BWPs from road vehicles in PM2.5 and PM10 sizes for year 2014.

Preprints (www.preprints.org) | NOT PEER-REVIEWED | Posted: 27 March 2020 doi:10.20944/preprints202003.0385.v1

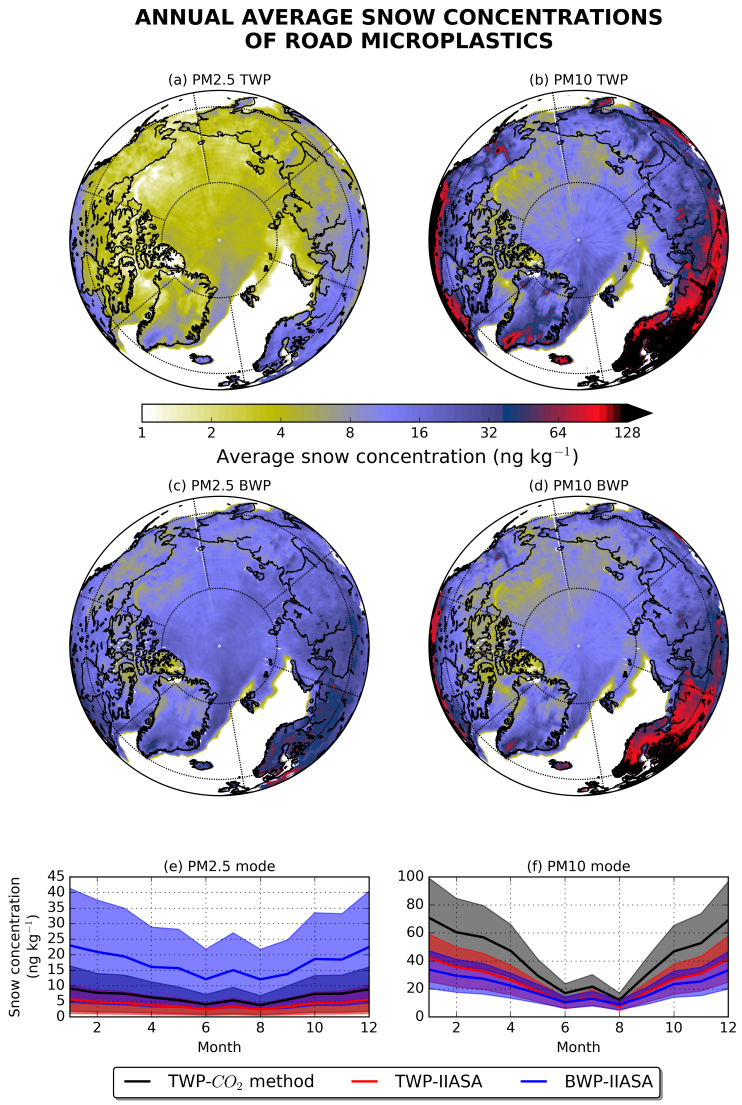

Fig. 3. Annual average concentrations of road microplastics in Arctic snow (a-d) in ng kg^{-1}. Snow concentrations were calculated using daily fields of sea-ice area fraction and total snowfall from European Centre for Medium Range Weather Forecast (ECMWF) combined with daily modeled deposition. The latter includes results from 120 simulations that accounted for different airborne fractions (five members for each of the PM2.5 and PM10 fractions, **Methods**), particle size distribution (eight members for each of the PM2.5 and PM10 fractions, **Extended Data Fig. 3**) and CCN/IN efficiency (three different sets of scavenging coefficients per fraction, **Extended Data Table 1**) following a log-normal distribution (see **Methods** and **Fig. S 2**). Monthly variation of concentrations of road microplastics in the Arctic snow in both sizes (PM2.5 and PM10) are presented in panels e and f. For the latter, model results using emissions from both methods are presented. TWP and BWP uncertainties have been calculated as the geometric standard deviation of all the 120 simulations with different assumption (airborne fraction, size distribution and CCN/IN efficiency, see **Methods**). Note that the smallest concentrations occur in mid-summer (see panels e and f).

Preprints (www.preprints.org) | NOT PEER-REVIEWED | Posted: 27 March 2020 doi:10.20944/preprints202003.0385.v1

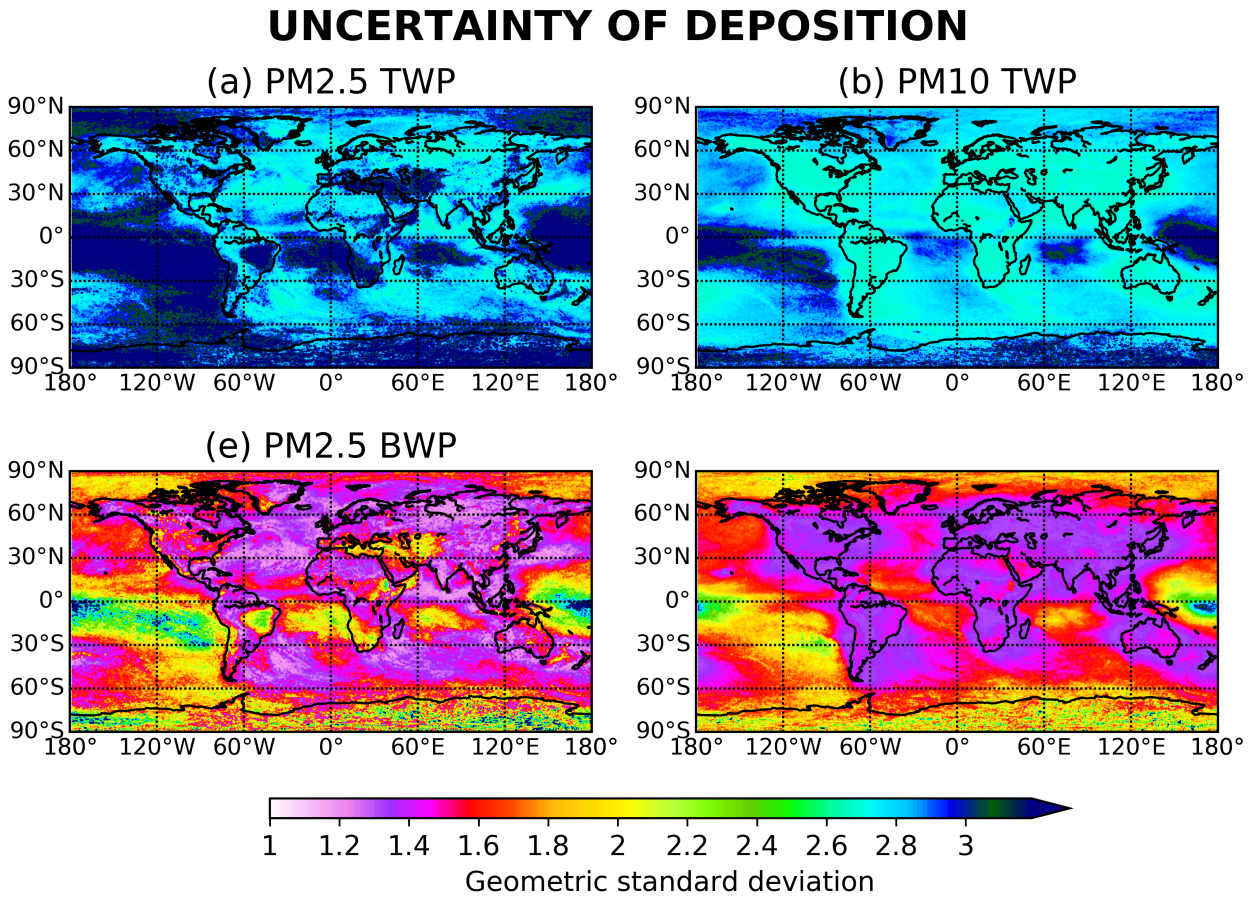

Fig. 4. Calculated model uncertainties of deposition. Uncertainties were calculated from a model ensemble of 120 members for each of the PM2.5 and PM10 sizes, both for TWPs and BWPs. The ensemble accounts for (a) airborne PM10 TWP fraction to be 2.5%, 5%, 10%, 20% and 40% of the total TWP emissions, PM2.5 TWP to be 0.25%, 0.5%, 1%, 2% and 4% of the total TWP emissions, while PM2.5 BWP fraction was assumed 30%, 40%, 50%, 60% and 70% of total BWPs and PM10 BWP fraction of 60%, 70%, 80%, 90% and 100% of the total BWPs (see **Methods**), (b) different wet scavenging coefficients that define CCN/IN efficiency, which are presented in **Extended Data Table 1** and (c) different assumptions on the airborne fraction in the emissions illustrated in **Extended Data Fig. 3** (see **Methods**). Uncertainties are given as the geometric standard deviations, since sensitivity scenarios followed a largely log-normal distribution (see **Methods** and **Fig. S 2**).

Preprints (www.preprints.org) | NOT PEER-REVIEWED | Posted: 27 March 2020 doi:10.20944/preprints202003.0385.v1

SUPPLEMENTARY VIDEO LEGENDS

The file contains five (5) video animations (mp4 format) and 12 figures, which have been created using the open access general-purpose programming language Python version 3.

Video S 1. Surface concentrations of TWPs (using emissions calculated with the CO2 ratio method and the GAINS model) and BWPs (GAINS model) in the PM2.5 and PM10 size modes (see **Methods**). Each panel is the geometric mean of 120 different simulations with different airborne fraction assumed (five members for each of the PM2.5 and PM10 fractions, **Methods**), different particle size distribution (eight members for each of the PM2.5 and PM10 fractions, **Extended Data Table 1**) and CCN/IN efficiency (three different sets of scavenging coefficients per fraction, **Extended Data Fig. 3**).

Video S 2. Monthly ratios of snowfall to total precipitation from ECMWF operational fields. We calculated snow concentrations for the grid-cells with non-zero snowfall and only for the months where snowfall was more than 90% of total precipitation. Snow concentrations are the geometric mean values of 120 model simulations that accounted for different airborne fraction (five members for each of the PM2.5 and PM10 fractions, **Methods**), particle size distribution (eight members for each of the PM2.5 and PM10 fractions, **Extended Data Table 1**) and CCN/IN efficiency (three different sets of scavenging coefficients per fraction, **Extended Data Fig. 3**) following a log-normal distribution (see **Methods** and **Fig. S 2**).

Video S 3. Global column integrated concentrations and accumulated deposition of TWPs in the PM2.5 and PM10 modes. Emissions were calculated using the CO_2 ratio method (see **Methods**). Each panel is the geometric mean of 120 different simulations with different airborne fraction assumed (five members for each of the PM2.5 and PM10 fractions), different particle size distribution (eight members for each of the PM2.5 and PM10 fractions) and CCN/IN efficiency (three different sets of scavenging coefficients per fraction) presented in detail in **Methods**, **Extended Data Table 1** and **Extended Data Fig. 3**.

Video S 4. Same as **Video S 3**, but using emissions from the GAINS model (IIASA) (see **Methods**).

Video S 5. Global column integrated concentrations and accumulated deposition of BWPs in the PM2.5 and PM10 mode using emissions from the GAINS model. Each panel is the geometric mean of 120 different simulations with different airborne fraction assumed (five members for each of the PM2.5 and PM10 fractions), different particle size distribution (eight members for each of the PM2.5 and PM10 fractions) and CCN/IN efficiency (three different sets of scavenging coefficients per fraction). All members are presented in detail in **Methods**, **Extended Data Table 1** and **Extended Data Fig. 3**.

SUPPLEMENTARY FIGURE LEGENDS

Fig. S 1. Monthly (12) snow concentrations of road microplastic particles in the Arctic snow. Total snowfall and snow depth were adopted from European Centre for Medium Range Weather Forecast (ECMWF). The concentrations were calculated using daily modelled deposition of road microplastics and daily fields of total snowfall (in m of water equivalent) from ECMWF operational fields and only over land (using a land-sea mask) and/or sea-ice (using sea-ice area

 doi:10.20944/preprints202003.0385.v1

fraction from ECMWF). The annual average snow concentrations were calculated only for months where snowfall was more than 90% of total precipitation (see **Methods**).

Fig. S 2. Probability density functions (PDF) of deposition of TWPs and BWPs for both PM2.5 and PM10 sizes. Note that PDF is based on a model ensemble of 120 members that includes five (5) members with different assumptions on the airborne fraction in the emissions (see **Methods**), eight (8) members assuming different particle size distribution in the atmospheric dispersion (**Extended Data Table 1**) and three (3) members with different scavenging coefficients expressing the CCN/IN efficiency (**Extended Data Fig. 3**).